

# Classification Tree for Material Defect Detection Using Active Thermography

Grzegorz Dudek<sup>(✉)</sup>  and Sebastian Dudzik 

Department of Electrical Engineering,  
Czestochowa University of Technology, Czestochowa, Poland  
{dudek, sebdud}@el.pcz.czest.pl

**Abstract.** Active thermography is a highly efficient and powerful technique that enables us to detect the subsurface defects by heating the investigated material sample and recording the thermal response using an infrared camera. In this work a simple variant of the time-resolved infrared radiometry method was used. The study was conducted for a sample made of the low thermal diffusivity material with artificially produced aerial defects. As a result of experiment, the sequence of thermograms was obtained. Heating and cooling curves for each thermogram pixel were determined and treated as patterns describing local features of the material. These patterns are recognized by classification tree and classified into two categories: “defect” or “non-defect”. Advantages of classification tree is an automatic feature selection and strong reduction of the pattern dimensionality. On the basis of simulation study, it can be concluded that classification tree is a useful tool for the characterisation and detection of material defects.

**Keywords:** Active thermography · Classification tree · Defect detection

## 1 Introduction

Non-destructive testing methods are used to detect material discontinuities (i.e. defects) without changing their properties [1]. This enables us to control the manufacture quality of the structural elements of devices, their components and even end products. Typical application areas of the non-destructive testing include:

- aerospace industry,
- automotive industry,
- chemical and petrochemical industries,
- conventional and nuclear power industry,
- railways,
- construction.

In non-destructive testing various methods are used to ensure the quality of products, e.g.: ultrasonic, radiological, eddy current, as well as the passive and active thermography [1, 2]. The presence of defect in subsurface material layer can be stated using a thermal wave theory [3, 4]. This theory plays a fundamental role in the defect detection with the active thermography methods. According to the theory, when we

subject a material sample to the periodic thermal extortion with amplitude  $T_{bA}$ , the temperature value at time  $\tau$  and at depth  $z$  can be described using a thermal wave equation [1]:

$$T(z, \tau) = T_{bA} \cdot \exp\left(-\frac{z}{\mu}\right) \cos\left(\omega \cdot \tau - \frac{2 \cdot \pi \cdot z}{\lambda}\right) \tag{1}$$

where:  $T_{bA}$  – amplitude of the periodic thermal excitation,  $\tau$  – time,  $z$  – depth,  $\mu$  and  $\lambda$  are the thermal diffusion length and thermal wave length, respectively, expressed as [5]:

$$\mu = \sqrt{\frac{2 \cdot \Lambda}{\omega \cdot \rho \cdot c_p}} = \sqrt{\frac{2 \cdot a}{\omega}}, \quad \lambda = 2\pi\mu \tag{2}$$

where:  $\Lambda$  – thermal conductivity of the material,  $\omega$  – thermal wave frequency,  $\rho$  – material density,  $c_p$  – material specific heat,  $a$  – thermal diffusivity of the material.

The active thermography relies on the heating of the investigated material surface and then recording the temperature field over the time [5–7]. Depending on the experimental procedure, various thermal excitation sources are used. In particular, there is possible to use the short energy pulse (pulsed thermography), periodically variable heating (lock-in thermography) and long pulse with a low energy (stepped heating). In each of these methods, a recording of the temperature field in the heating phase, cooling phase or both of them is conducted. The presence of defect is stated on the basis of the analysis of recorded temperature field. Different methods are used for this case: methods based on the modelling of the heat transfer occurred in the investigated material sample, digital processing methods or machine learning methods [5–8]. As a result of the stepped heating method, data vectors with multiple features (representing temperatures) are obtained. Therefore dimensionality reduction methods (e.g. PCA) are required for classification purposes [8]. In this paper the classification tree is used to analyze the sequence of thermograms. This method is equipped with built-in feature selection mechanism, which is a valuable advantage in this application.

From the point of view of the experimental practice, the lock-in and the pulse methods can be difficult to apply [1]. Therefore, in this work, a simple variant of the time-resolved infrared radiometry method was used [1, 5]. In this variant, the geometry of investigated sample is described by a two-layer model, wherein the second layer, denoted as L2, represents a subsurface defect (Fig. 1).

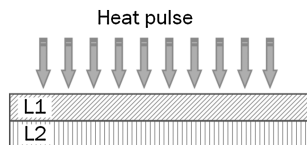


Fig. 1. Two-layer model of the investigated sample.

During the experiment, a temperature rise is monitored over the all excitation period (i.e. the sample under investigation is constantly heated at low power for a specified time). Eventually, as the result of experiments, the thermal image sequence (the sequence of thermograms) is obtained.

In this work, on the basis of sequence of thermograms the heating-cooling curves (H-CCs) are determined and analyzed. The classifier using the classification tree is proposed to recognize “defect” and “non-defect” areas of the sample. The input patterns of the tree are H-CCs.

The remaining sections of the paper are organized as follows. In Sect. 2, experimental investigations using active thermography are described. Section 3 presents a classification tree for defect detection on the basis of thermograms. In Sect. 4, we analyze the thermograms and evaluate the performance of the classification tree. Finally, Sect. 5 is a summary of our conclusions.

## 2 Experimental Investigations Using Active Thermography

The active thermography experiments were conducted with an experimental setup presented in Fig. 2.

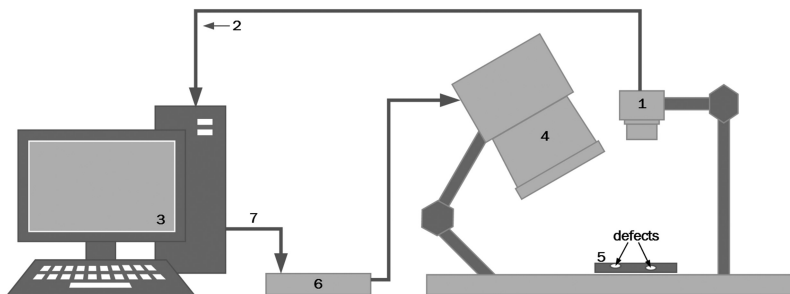


**Fig. 2.** The experimental setup used in the active thermography investigations.

The setup comprises of:

1. Long-wave infrared camera IRS336-NDT (FPA detector, spatial resolution: 336256 pixels, NETD < 50 mK) used to record the thermal image sequence.
2. Digital interface GigEVision with GenICam used for linking the camera with PC.
3. PC equipped with the software for data acquisition and processing. It cooperates with the heat excitation controller and the infrared camera.
4. Halogen lamp with 2.0 kW power equipped with a power amplifier controlled by a heat excitation controller.
5. Sample under investigation contained artificial defects.
6. Heat excitation controller.
7. USB cable.

The sample under investigation was made of Plexiglas. Nine blind flat-bottomed holes at different depths were drilled in the sample. The holes are made with different diameters ranging from 2.0 mm to 3.4 mm. The thickness of the sample was equal to 10 mm. To avoid the effect of an external radiation, the heated surface of the sample was covered with a paint of high band emissivity coefficient ( $\varepsilon \approx 0.95$ ). A scheme of the investigated sample geometry is shown in Fig. 3.

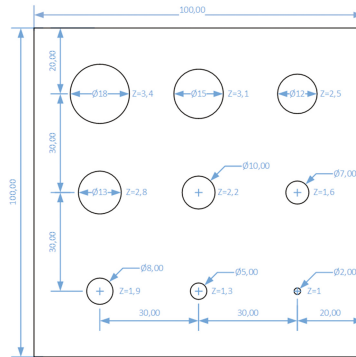


**Fig. 3.** The scheme of the investigated sample geometry (each dimension in mm)

In the experiments the surface of the sample was heated with a halogen lamp for a 120 s with 70% power. At the same time the sequence of thermal images was recorded using the infrared camera. The recording was conducted at frame rate equals to 5 Hz. Further, the cooling phase lasting 80 s without the lamp excitation was recorded as well. As a result of experiment, the sequence of 1000 thermograms was obtained. Each thermogram consists of  $211 \times 212$  pixels.

Some examples of thermograms of the surface of investigated sample in Fig. 4 are shown. They were recorded after time  $\tau = 20$  s (early heating phase),  $\tau = 120$  s (end of the heating phase) and  $\tau = 199$  s (late cooling phase). Analysing the results shown in Fig. 4, you can observe the blur of the imaged defects, which is strongly dependent on the time instant of recording. The blur is due to the nature of the heat transfer process occurred in the investigated sample. Inside the sample the heat flows in all directions, including the plane parallel to the surface under investigation. It affects the change in surface temperature distribution. Between defect and non-defect areas the heat flow is disturbed and the transition zones appear. The presence of the zones can cause problems at the data processing stage, especially when the transition pixels should be used as a source for the training data in machine learning routines.

In Fig. 5 the H-CCs are shown measured in two points representing “defect” and “no defect” classes. As can be seen from this figure the curve of class “defect” is above the curve for class “non-defect”. This is because of the lesser local heat capacity in the defect points, where the material layer is thinner. This phenomenon can be used for defect detection. In the next section classification tree is proposed, which classify H-CCs and thus recognizes defect regions.

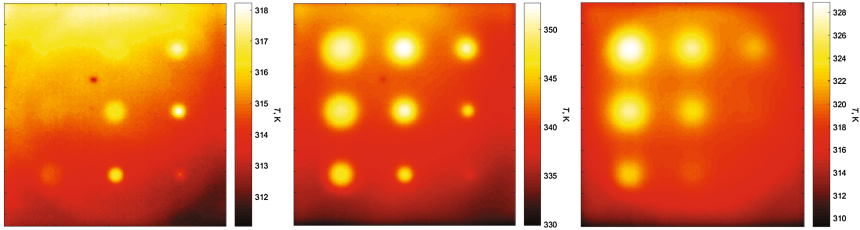


**Fig. 4.** Thermograms of the surface of investigated sample recorded at  $\tau = 20$  s (left),  $\tau = 120$  s (middle), and  $\tau = 199$  s (right).

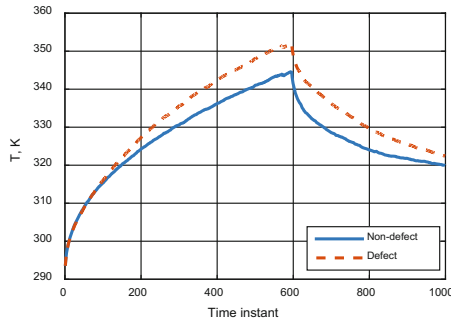


**Fig. 5.** The heating-cooling curves representing “defect” and “non-defect” classes.

### 3 Classification Tree for Defect Detection

Decision trees are popular tools of machine learning used for inductive inference. They approximate a target function discretely and represent it in a tree structure or alternatively in the set of IF-THEN decision rules. The advantage of decision trees over other methods of data classification and function fitting, e.g. neural networks, are their direct interpretability (clear logical rules implemented in the tree) and the ability to act not only on quantitative but also qualitative (nominal and ordinal) variables.

We focus on the variant of decision trees proposed by Breiman [9] called CART (Classification and Regression Trees). In our case CART learns to solve the classification problem, where the response variable  $y$  is a class symbol: “defect” or “non-defect”. Input patterns are vectors  $\mathbf{x} \in \mathbb{R}^n$  representing H-CCs. The successive components of  $\mathbf{x}$  are temperatures at successive time instants. Each thermogram pixel is represented by a pair  $(\mathbf{x}, y)$ , where  $\mathbf{x} = [T_1 T_2 \dots T_n]$  is a H-CC measured for this pixel, and  $y \in \{\text{“defect”}, \text{“non-defect”}\}$ . For  $N$  pixels we have a set of  $N$  training instances  $\Omega = \{(\mathbf{x}_i, y_i), (\mathbf{x}_i, y_i), \dots, (\mathbf{x}_N, y_N)\}$ .

An example of classification tree is shown in Fig. 6. The tree consists of intermediate nodes (marked with triangles), which perform tests on input variables (components of  $\mathbf{x}$ ), terminal nodes (leaves; marked with points) with labels indicating a class, and branches connecting nodes. CART is a binary tree, i.e. each intermediate node has only two children.

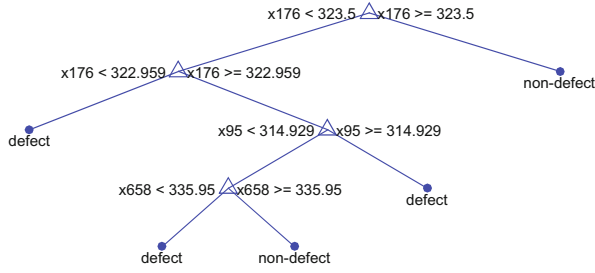


**Fig. 6.** Example of CART.

The tree is constructed with a top-down induction algorithm (recursive tree-growing process). In the intermediate nodes the set of instances is split into two subsets: positive instances that meet the test assigned to the node, and negative ones that do not meet this test. In the case of continuous variables this is an inequality test of the form:

$$\chi(\mathbf{x}) = \begin{cases} 1, & \text{if } x_i < s_i \\ 0, & \text{if } x_i \geq s_i \end{cases} \quad (3)$$

where  $x_i$  is a splitting variable and  $s_i$  is a split-point.

The splitting variables and split points are selected using the a greedy algorithm which tests all variables (1000 successive temperature values of the H-CC in our case) and all possible split-points. The best split is selected, which maximizes the drop in impurity of the node defined by:

$$\Delta I_i = I - p_L I_L - (1 - p_L) I_R \quad (4)$$

where  $I$  is an impurity of the parent node,  $I_L$  and  $I_R$  are the impurities of the left and right children nodes, and  $p_L$  is the fraction of instances that will go to the left node when test  $\chi$  is used.

As an impurity measure Gini’s diversity index is used, which for two classes is defined as:

$$I = 2q(1 - q) \quad (5)$$

where  $q$  is the observed fraction of instances that are in category “defect”.

The stopping rule is: the node is pure (it contains only instances of one class) or there is no reduction in impurity or there are fewer than  $L$  instances in the node. When a node meets one of these conditions it becomes a leaf. The parameter  $L$  controls the depth of the tree. Deeper trees with many leaves are usually highly accurate on the training data, but tend to overfit. They are not guaranteed to show a comparable accuracy on a test set. Shallow trees can be more robust and easy to interpret.

## 4 Simulation Study

In this section we analyze the thermograms for the sample fragment of  $39 \times 39$  pixels around the middle hole  $\phi 10$ . In Fig. 7 the H-CCs recorded for all 1521 pixels are shown. They form two overlapped bands: upper band including curves for defect pixels and lower band including curves for non-defect pixels. Pixels for which H-CCs lie in the overlapping region can be unrecognized. As we can see from Fig. 7 the overlapping band is not very wide. A narrow overlapping band means that the classes are well separated, and that the temperature has a great discriminative power, i.e. the ability to separate classes “defect” and “non-defect”. But the width of the overlapping band is dependent on the time. This is shown in Fig. 8 presenting the number of pixels lying in the overlapping region. For lower time instants the classes are poorly recognizable because most of 1521 pixels lie in the overlapping region. For time instants greater than about 100 the number of pixels in overlapping region decreases rapidly to several dozen or even a dozen or so.

In Fig. 9 the thermograms recorded at time instant 50 ( $\tau = 10$  s), 100 ( $\tau = 20$  s), and 600 ( $\tau = 120$  s) are shown. The pixels within the defect area are marked with black dots. Pixels lying in overlapping region are marked with rings. As can be seen from this figure for  $\tau = 10$  s pixels from the upper part of the thermogram and pixels from the defect area lie in the overlapping region. Their temperatures are very similar. After a time of  $\tau = 20$  s, the differences in temperatures between “defect” and “non-defect” pixels are more distinct. Temperatures in “defect” pixels are higher than in “non-defect” ones. The pixels from the transition zone between defect and non-defect areas lie in the overlapping region. There is 74 of such pixels. After  $\tau = 120$  s their number is reduced to 18. Thus, the temperature has the higher discriminative power for  $\tau = 120$  s than for 10 and 20 s.

Classification tree constructed for defect detection on the basis of thermograms in Fig. 10 is shown. The training set consisted of 1521 labeled x-patterns representing H-CCs for each pixel. The classification error estimated using 10-fold cross-validation was 0.53%. As we can see from Fig. 10 only three points of the curves were selected as splitting variables:  $T_{776}$ , i.e. the temperature recorded after the time  $\tau = 155.2$  s,  $T_{73}$ ,

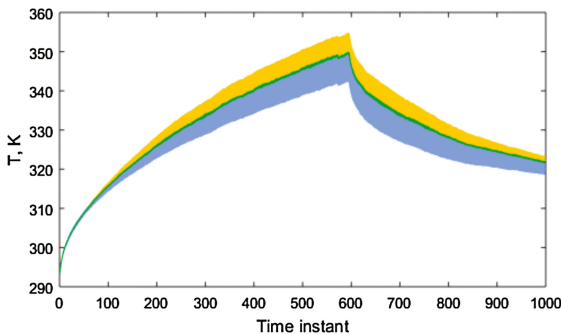


**Fig. 7.** The heating-cooling curves representing “defect” (upper band) and “non-defect” (lower band) classes for all pixels.

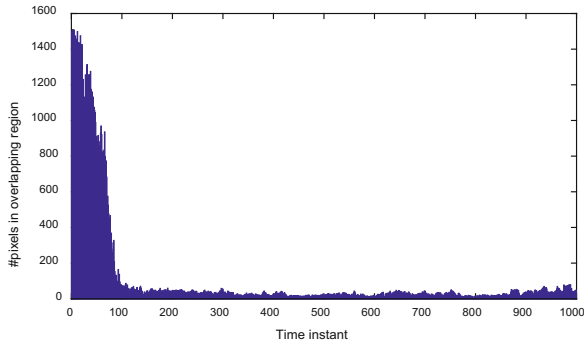


**Fig. 8.** Number of pixels for which the heating-cooling curves lie in the overlapping band.

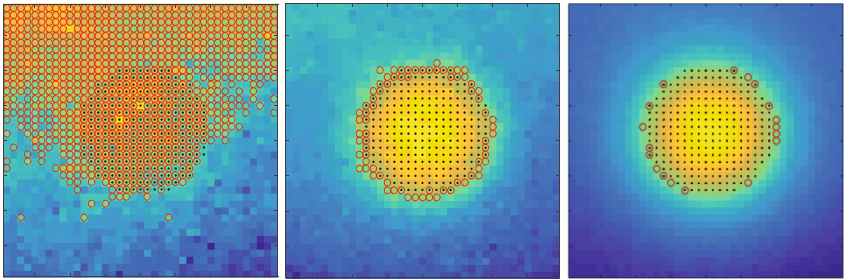


**Fig. 9.** Thermograms recorded at time instant 50 (left), 100 (middle), and 600 (right). Defect area are marked with black dots. Pixels lying in overlapping region are marked with rings.

i.e. the temperature recorded after the time  $\tau = 14.6$  s, and  $T_{138}$ , i.e. the temperature recorded after the time  $\tau = 27.6$  s. The embedded mechanism of variable selection is a valuable property of decision trees. Note that for classification new instances we do not need to provide entire H-CCs but only three temperature values.

The training set of 1521 instances was split in the root node using  $T_{776}$  into left subset containing 1250 instances of “non-defect” class, and right subset containing 268 instances of “defect” class and 3 of “non-defect” class. The right subset is further split using  $T_{73}$  into left subset having only two “non-defect” instances, and right subset having 268 “defect” instances and one “non-defect” instance. Finally, the right subset is split using  $T_{138}$  giving two leaves with one “non-defect” instance and 268 “defect” instances. Note that all leaves of the tree are pure.

The division of the training set in Fig. 11 is shown. The vertical line represents split-point for  $T_{776}$ , which almost perfectly separates two classes. The horizontal line represents split-point for  $T_{73}$ , which separates two “non-defect” instances from the rest of the data. Third split using  $T_{138}$  (not shown in the figure) separates one “non-defect” instance from 268 “defect” ones.

In the last experiment we test how the reduction in the x-pattern length to  $m < n$  first components will affect the classifier accuracy. Now patterns  $\mathbf{x}$  include the

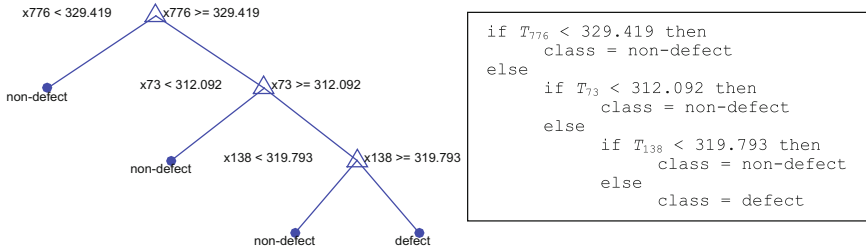


**Fig. 10.** Optimal CART and decision rules expressing the tree.

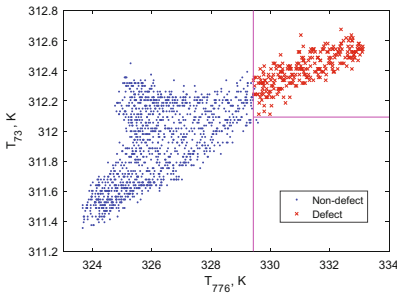


**Fig. 11.** Training data divided into classes by CART.

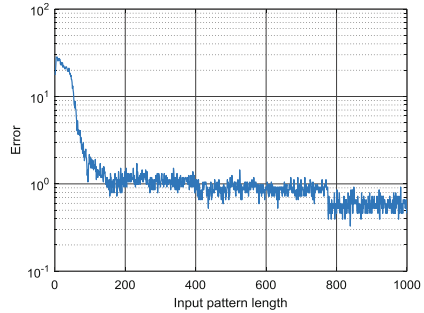


**Fig. 12.** Classification error depending on the input pattern length.

first parts of H-CCs, from  $T_1$  up to  $T_m$ . Figure 12 shows classification error depending on  $m$ . When  $m$  is too small the temperatures measured on the surface of the sample do not allow the tree to distinguish between classes. For  $m > \sim 150$  the error decreases to about 1%, and stays at that level up to  $m = 776$ . Then the error unexpectedly jumps to the level of about 0.5%, which is rather accidental.

## 5 Conclusion

In this work, we have demonstrated on the basis of simulation studies that the thermal characteristics of the sample, i.e. the heating-cooling curves, are good information carriers about the subsurface defects in the material. A classification tree used for defect detection gave very low errors, even for short sequences of thermograms including beginning of the heating phase (not less than 30 s). But it should be remembered that our research concerned a simplified case: a fragment of a sample with only one distinct defect, where the area of defect is close to the area of non-defect (balanced case). In real applications, where there are many different defects, which total area is much smaller than the area of the material, higher errors should be expected.

The recursive tree-growing process has embedded mechanism of feature selection, which allowed the tree to select only three points of the heating-cooling curve out of a

thousand to classify perfectly all thermogram pixels as “defect” or “non-defect”. This automatic selection of the most informative variables, as well as interpretability (a tree can be expressed as a logical expression which is human understandable) and rapid classification are very suitable for material defect detection using active thermography.

## References

1. Maldague, X.P.: *Theory and Practice of Infrared Technology for Nondestructive Testing*. Wiley, Interscience, New York (2001)
2. Minkina, W., Dudzik, S.: *Infrared Thermography – Errors and Uncertainties*. Wiley, Chichester (2009)
3. Fourier, J.: *Théorie du mouvement de la chaleur dans les corps solides – 2 Partie*. Mémoires de l'Académie des Sciences **5**, 153 (1826)
4. Ångström, M.A.J.: New method of determining the thermal conductivity of bodies. *Phil. Mag.* **25**, 130–142 (1863)
5. Dudzik, S.: Estimation of the material defects depth using an active thermography and artificial neural networks, Częstochowa University of Technology Publishers, Częstochowa (2013, in Polish)
6. Dudzik, S.: Application of the naive Bayes classifier to defect characterization using active thermography. *J. Nondestr. Eval.* **4**(31), 383–392 (2012)
7. Dudzik, S.: Two-stage neural algorithm for defect detection and characterization uses an active thermography. *Infrared Phys. Technol.* **71**, 187–197 (2015)
8. Dudzik, S.: Analysis of the accuracy of a neural algorithm for defect depth estimation using PCA processing from active thermography data. *Infrared Phys. Technol.* **56**, 1–7 (2013)
9. Breiman, L., Friedman, J.H., Olshen, R.A., Stone, C.J.: *Classification and Regression Trees*. Wadsworth, Monterey (1984)